Electronic structure and dispersion of compensated *n-i-p-i* superlattices with small period lengths

J. Y. Lin and H. X. Jiang*
Department of Physics, Kansas State University, Cardwell Hall, Manhattan, Kansas 66506
(Received 13 March 1989)

A detailed calculation of energy-band structures and dispersion relation of compensated *n-i-p-i* superlattices with small period lengths is presented. The calculation is based on a multistep-function approach to the real potential form and the transfer-matrix method. The densities of states of conduction subbands have been calculated. We found that the density of states is different for different subbands. Some special features of small-period doping superlattices have been explored, and are compared with properties of long-period *n-i-p-i* compensated doping superlattices as well as GaAs-$Al_xGa_{1-x}As$ compositional superlattices.

I. INTRODUCTION

Recently, quantum wells and superlattices have attracted a great deal of attention because of their novel properties.[1,2] The availability of this class of semiconductor structures creates new avenues for the investigation of the physics of condensed matter under conditions of greatly reduced dimensionality where quantum effects become apparent, thus extending the underlying physics to totally new fundamental phenomena. These structures are also important materials for various device applications such as high-speed electronics, optoelectronics, and photonic devices.

There are two types of superlattices with alternating ultrafine layers: doping and compositional. The compositional superlattices are composed of a periodic sequence of alternating layers of two different kinds of compositional materials. They have been investigated extensively during the past few years. Among these, the GaAs-$Al_xGa_{1-x}As$ superlattices have been most studied. The *n-i-p-i* superlattices consist of a periodic sequence of ultrathin layers of alternating doping [e.g., (n-type GaAs)/(p-type GaAs)]. Despite the wealth of optical and electrical properties discovered over the recent years, *n-i-p-i* superlattices are much less understood compared with compositional superlattices.

Since the first careful theoretical investigation on doping superlattices[3-5] there have been many theoretical and experimental works in this field.[6,7] The energy bands in doping superlattices are due to the space-charge-induced band-edge modulation rather than the band-gap variation as in compositional superlattices, which leads to an indirect energy gap in real space. Thus, electron and hole states are spatially separated from each other. This is the origin of the fascinating tunabilities of many physical properties of doping superlattices, such as effective energy gap, absorption coefficient, photoluminescence, and electroluminescence, etc. These unique features show a promising future for doping superlattices in practical applications.

Most previous works in this field have emphasized, explicitly or implicitly, on doping superlattices with long period lengths ($L > 500$ Å). The subband structures of *n-i-p-i* superlattices have remained obscure for a long time. Instead, the harmonic-oscillator-type energy levels have been widely used to approximate the electron (hole) energy levels in the imposed periodic potential wells.[3-5] In fact, many special features, such as the tunability of the effective energy gap, greatly depend on the long carrier lifetime ($t \sim 1000$ sec), which is the direct consequence of the spatial separation of electron and hole states, and the negligible tunneling probability between adjacent wells. The latter requires a long period length, which leads doped layered structures to be essentially decoupled multiple quantum wells.

Experimentally, there were some limiting factors for the growth of doping superlattices with thin periods due to the solubility limit of impurities in the homogeneous doping process. However, with the newly developed δ-doping technique,[8] Schubert *et al.*[9] were able to obtain small-period doping superlattices with sawtooth-shaped conduction- and valence-band edges. They discovered some new electronic and photoluminescence properties for small-period (~ 100 Å) *n-i-p-i* superlattices. Recently, Yan and Jiang[10] calculated the dispersion of electronic subbands is compensated *n-i-p-i* superlattices by accurate numerical computation. It was shown that the minibands of *n-i-p-i* superlattices of the small period length have finite widths, and the dispersion is comparable to that of GaAs-$Al_xGa_{1-x}As$ compositional superlattices of the same period. Therefore, for small-period *n-i-p-i* superlattices, the approximation of oscillator-type energy levels to subbands is no longer adequate. Since many unique properties of superlattices are closely related to the subband structures, detailed and careful investigation of these structures are essential.

In this paper, we describe a detailed method of calculation of the subband structures and dispersion of compensated *n-i-p-i* superlattices. The effective energy gaps of heavy and light holes, are also investigated. The density of states are obtained from the dispersion relation. Some unique properties are explored.

II. CALCULATIONS

A n-i-p-i superlattices is a periodic sequence of ultrathin n-type and p-type doped layers with intrinsic layers in between. The imposed periodic potential is caused by the positively charge ionized donors in the n-type layers and the negatively charged acceptors in the p-type layers. In the calculation, we assume that the doping is homogeneous, i.e., the doping concentration n_D and n_A are constants in the respective doping layers. The potential fluctuations, which arise from the statistical distribution of the dopants in the layer and the point-charge character of the impurities, have been neglected. The effects of the point-charge character of the impurities have been discussed in Ref. 3. The authors concluded that the effects on the electrons are negligible. Furthermore, we should restrict ourselves in the case of the compensated doping semiconductor superlattices, which requires $n_D d_n = n_A d_p$, where d_n and d_p are the thicknesses of n- and p-type layers, respectively. In this case, by integrating the Poisson's equation, we get the periodic space-charge potential as

$$V(z)=V_0(z-mL), \quad -L/2 \le z-mL < L/2 \tag{1}$$

with $m=0,\pm1,\pm2,\ldots$, and z along the growth direction, and

$$V_0(z)=\frac{2\pi e^2}{\epsilon}\times\begin{cases} n_D z^2, & |z|\le d_n/2 \quad (2a)\\ n_D d_n(|z|-d_n/4), & d_n/2<|z|\le d_n/2+d_i \quad (2b)\\ n_D d_n(d_n/4+d_i)-n_A[(L/2-|z|)^2-d_p^2/4], & d_n/2+d_i<|z|\le L/2\ . \quad (2c)\end{cases}$$

Here d_i is the thickness of the intrinsic layer. The period length is thus $L=d_n+d_p+2d_i$. This form of periodic potential makes an exact analytic solution of the Schrödinger equation unfeasible. There have, however, been several attempts in trying to solve the Schrödinger equation numerically with various shapes of potential.[11–13] Of those, Ando and Ithoh[13] proposed a multistep-function approach to an arbitrary potential form and calculated the transmission tunneling current across the potential. This method turns out to be very simple and, nevertheless, easy to achieve high accuracy. We have applied this method to the periodic potential of Eq. (2) and calculated the corresponding band structures by the transfer-matrix method.[14]

Figure 1(a) shows the band profile of the compensated n-i-p-i semiconductor superlattice with $d_i=d_n=d_p=L/4$. Figures 1(b) and 1(c) show the potential of Eq. (2) with the approximation of the multistep functions with 40 and 200 steps in one period, respectively. They can be expressed as

$$V(x)=V_j=V[(z_{j-1}+z_j)/2]\ , \tag{3}$$

$$m^*(x)=m_j^*=m^*[(z_{j-1}+z_j)/2]\ , \tag{4}$$

for $z_{j-1}<z<z_j$, $j=0,1,2,\ldots,N$, where N is the total number of steps in one period. Here z_j is the coordinate for jth step and m^* is the effective mass of electrons or holes. For $N=40$, the difference between the real potential and multistep-potential approximation in Fig. 1(b) is obvious. However, as the total steps in each period approach to $N=200$ in Fig. 1(c), the difference between the real potential and multistep-potential approximation cannot easily be distinguished. So the results obtained here can represent the exact solution. With the multistep-potential approach, the wave function Ψ_j^n in the jth step region of the nth period can be written as

$$\Psi_j^n(z)=A_j^n\exp(ik_jz)+B_j^n\exp(-ik_jz)\ , \tag{5}$$

where

$$k_j=[2m_j^*(E-V_j)]^{1/2}/\hbar\ ,$$

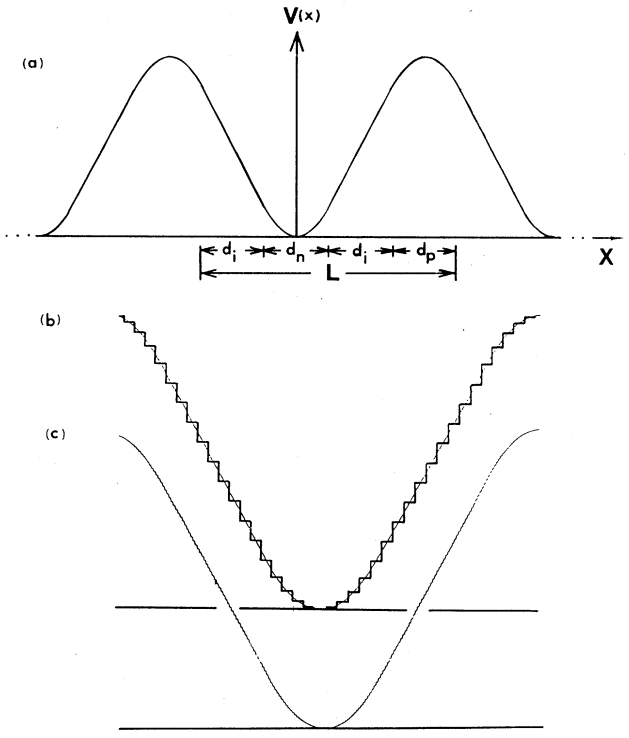

FIG. 1. (a) Schematic of the space-charge potential of a compensated n-i-p-i semiconductor superlattice with $d_i=d_n=d_p=L/4$; L is the period length. (b) and (c) are the approximation by the multistep functions with a total of 40 and 200 steps in each period, respectively.

where k_j can be real or imaginary depending on whether energy E is larger or smaller than the jth step potential V_j. Using the continuity conditions of wave functions and its derivative at the interfaces of adjacent steps, we have

$$\begin{bmatrix} A_j^n \\ B_j^n \end{bmatrix} = \prod_{i=0}^{j-1} \underline{M}_i \begin{bmatrix} A_0^n \\ B_0^n \end{bmatrix}, \tag{6}$$

where

$$\underline{M}_i = \frac{1}{2} \begin{bmatrix} (1+S_i)\exp[-i(k_{i+1}-k_i)z_i] & (1-S_i)\exp[-i(k_{i+1}+k_i)z_i] \\ (1-S_i)\exp[i(k_{i+1}+k_i)z_i] & (1+S_i)\exp[i(k_{i+1}-k_i)z_i] \end{bmatrix}, \tag{7}$$

and

$$S_i = \frac{m_{i+1}^*}{m_i^*} \frac{k_i}{k_{i+1}} .$$

For simplicity, we assume that the effective mass is the same everywhere in the system, then we have $S_i = k_i/k_{i+1}$. Note that

$$A_0^n = A_N^{n-1} e^{ik_{N-1}L}, \quad B_0^n = B_N^{n-1} e^{-ik_{N-1}L},$$

and so

$$\begin{bmatrix} A_N^n \\ B_N^n \end{bmatrix} = \underline{M} \begin{bmatrix} A_N^{n-1} \\ B_N^{n-1} \end{bmatrix} = \underline{M}^n \begin{bmatrix} A_N^0 \\ B_N^0 \end{bmatrix}, \tag{8}$$

with

$$\underline{M} = \begin{bmatrix} M_{11} & M_{12} \\ M_{21} & M_{22} \end{bmatrix} = \prod_{i=0}^{N-1} \underline{M}_i \begin{bmatrix} e^{ik_{N-L}} & 0 \\ 0 & e^{-ik_{N-1}L} \end{bmatrix}. \tag{9}$$

From Eqs. (6) and (7), the determinant of matrix $\underline{M}$ is unity, $\det|\underline{M}| = 1$, and from the requirement that the wave function of the electron (hole) must be finite, we can define a real parameter q, which is related to the energy by the equation[14]

$$\cos(qL) = \tfrac{1}{2}\mathrm{Tr}(\underline{M}) . \tag{10}$$

Equations (7), (9), and (10) give the dispersion relation of the system. With increasing N, Eq. (10) approaches the exact solution of the system. Practically, with 200 steps in each period, we can obtain results of sufficient accuracy. The results presented in this paper are obtained with $N = 200$.

III. RESULTS AND DISCUSSIONS

In this paper, the calculations are performed for the compensated n-i-p-i GaAs superlattices. The dielectric constant ϵ and electron effective mass are 12.5 and $0.067m_0$, respectively.[15,16] Effective masses of heavy and light holes are $0.45m_0$ and $0.08m_0$, respectively, where m_0 is the electron mass in free space. The energy gap of GaAs has been taken as 1.520 eV.[16]

Figure 2 shows the dispersion of the first conduction band for a GaAs n-i-p-i superlattice (— — —) with $n_D = n_A = 10^{18}/\mathrm{cm}^3$, $d_i = d_n = d_p = L/4$, and $L = 120$ Å. For comparison, the dispersion of the same band for a GaAs-$Al_{0.3}Ga_{0.7}As$ compositional superlattice of equal well and barrier widths, $a = b = L/2$, and $L = 120$ Å, is shown as a solid line. The result of compositional superlattice is obtained by using the empirical expression, $E_g = 1.155x + 0.37x^2$ eV, as the direct band-gap difference between GaAs and $Al_xGa_{1-x}As$ materials.[17,18] The conduction-band offset at the interface of GaAs and $Al_xGa_{1-x}As$ has been taken as 60% of the direct-band gap difference between the two semiconductor materials,[19,20] and the effective mass of electron in the $Al_xGa_{1-x}As$ was taken as $m = (0.067 + 0.083x)m_0$.[17]

From Fig. 2, we can see that the dispersion of the n-i-p-i superlattice is quite different from that of the GaAs-$Al_xGa_{1-x}As$ compositional superlattice. The ground-state energy of electrons in the n-i-p-i superlattice is much lower than that in the corresponding compositional superlattice. In our case, the ground-state energies of electrons in n-i-p-i and compositional superlattices are about 4.6 and 71.7 meV, respectively. The bandwidth of the first conduction band of the doping superlattice (~37.2meV) is more than 1 order of magnitude larger than that of compositional superlattices (~2.9 meV). This is the direct consequence of the weaker electron confinement (also true for hole) in the doping superlattice than in the compositional superlattice. Therefore, the coupling effects due to the adjacent layers are much more important in doping superlattices in this case. Another important feature can be distinguished between these two superlattices, which is the wave-vector depen-

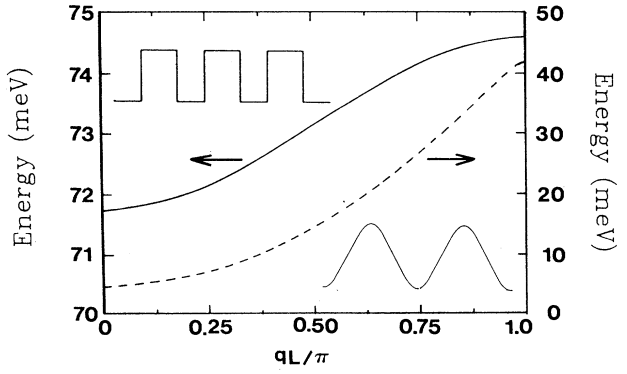

FIG. 2. Comparison of dispersions of the first conduction band for a GaAs n-i-p-i superlattice (— — —) at $n_D = n_A = 10^{18}$ cm^{-3}, $d_i = d_n = d_p = L/4$ and $L = 120$ Å with a GaAs-$Al_{0.3}Ga_{0.7}As$ compositional superlattice (——) of equal well and barrier widths, $a = b = L/2$ and $L = 120$ Å.

dence of the effective mass, i.e., $1/m^* = (1/\hbar^2) d^2E/dk^2$. For a doping superlattice, the dispersion is almost a parabolic curve except for a small region near the band edge ($0.95\,\pi < qL < 1.0\pi$). From the observation, we may conclude that the effective mass of the electron in a doping superlattice is almost constant in the entire band (independent with wave vector, q). However, the electron effective mass of a compositional superlattice strongly depends on the wave vector q. It changes from a positive value near the center of the band to a negative value near the band edge. In the region of $0.40\pi \leq qL \leq 0.60\pi$, the dispersion is almost a linear curve, which indicates that the effective mass is very large in this region.

Figure 3 is the plot of the first two conduction bands (shaded area) as functions of doping concentration n at $d_i = d_n = d_p = L/4$, $L = 160$ Å, and $n_D = n_A = n$. Electron energies are measured from the bottom of the potential wells. The most significant feature observed here is that the center of the band and the edge of the band have different doping concentration dependencies. This is especially evident for the first conduction band. The results obtained here are useful for interpreting photoluminesence experimental observations. At low temperatures, with increasing the population of photoexcited carriers, the density of ionized impurities decreases due to capture of carriers, and consequently the effective doping concentration decreases. Results in Fig. 3 show that electron energies in the conduction band with respect to the bottom of the potential wells decrease with decreasing the doping concentration. However, the effective energy gap, which is the energy difference between the minima of the first conduction and valence minibands, is significantly increased as the doping concentration is decreased. This is the consequence of decreased amplitude of the space-charge potential with decreasing n. Therefore, experimentally observed luminescence emission peaks shift towards higher energies when the excitation photon intensity is increased.[4] Results in Fig. 3 indicate that, besides the dominant effect of the space-charge potential variation caused by changing of the ionized-impurity concentration, the luminescence photon-energy shift is also affected by the electron Fermi level changing with excitation intensity. Additionally, results in Fig. 3 also modify the time-resolved luminescence spectral shape of n-i-p-i doping superlattices. In general, during the decay process, the concentration of ionized impurities in the respective layers increases with increasing the delay time due to carrier recombination. For long-period n-i-p-i doping superlattices, the band structures are almost dispersionless, and thus the variation in time-resolved emission spectra due to the Fermi level shifting is negligible. In contrast, for short-period n-i-p-i doping superlattices, one has to consider the fact that the Fermi levels shift towards the bottom of the potential well as the delay time increases. The relative decrease in the Fermi level may reach a value in the order of 10 meV for short-period doping superlattices, and thus the filling-states effect[21,22] cannot be neglected. Another feature in Fig. 3 is that widths of allowed conduction bands increase with decreasing the doping concentration, while minigaps decrease and approach zero at $n = 0$. This is because as n decreases, the amplitude of the space-charge potential decreases, and thus reduces the confinement of electrons, and therefore, the dispersion (or bandwidth) increases. In contrast, this effect was never discussed for long-period doping superlattices since they have negligible dispersions in minibands.

We also calculated the effective energy gap as a function of period length L. The result is depicted in Fig. 4, where the doping concentration was chosen to be $n_D = n_A = 10^{18}$ cm^{-3} and $d_n = d_p = d_i = L/4$. The solid (——) and dotted (— — —) lines represent the effective energy gaps of heavy and light holes, respectively. In the

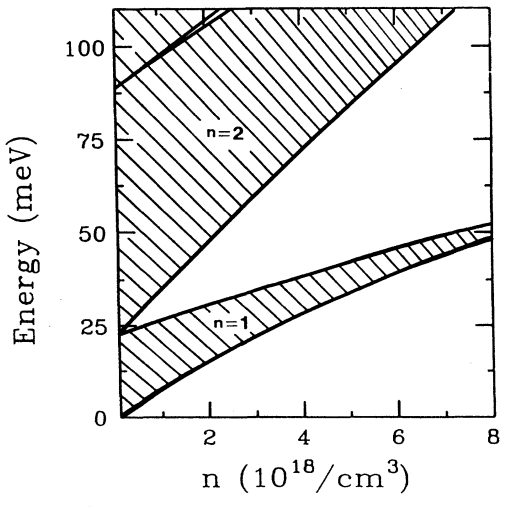

FIG. 3. The first two allowed conduction minibands (shaded area) and minigaps as functions of doping density ($n_D = n_A = n$) with $d_i = d_n = d_p = L/4$ and $L = 160$ Å.

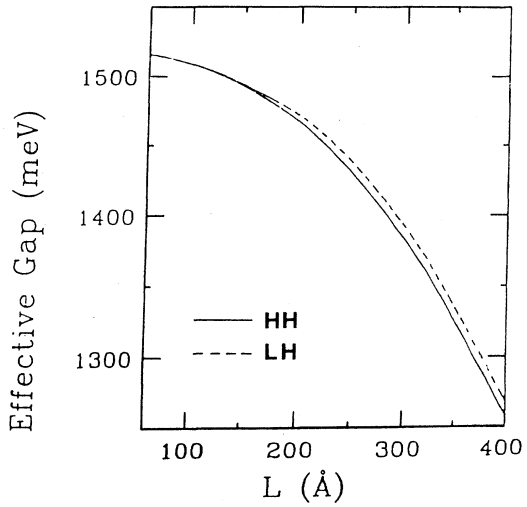

FIG. 4. Effective energy gaps of heavy (——) and light (— — —) holes as functions of period length L with $n_D = n_A = 10^{18}$ cm^{-3}, $d_i = d_n = d_p = L/4$.

calculation, the effect of mixing of light- and heavy-hole bands has been neglected. As in the compositional superlattices, the effective energy gap for light holes is larger than that of heavy holes. The effective energy gap also represents the minimum energy required for creating excitons if one neglects the Coulomb and phonon interactions. One must notice here that in n-i-p-i doping superlattices, the space-charge induced band-edge modulation rather than the band-gap variation in compositional superlattices, leads to an indirect energy gap in real space. A quantitative value of the exciton binding energy in n-i-p-i doping superlattices is unknown at this stage. In order to obtain the exciton binding energy, one has to solve the Schrödinger equation for electron-hole pairs in the presence of the modulation potential of Eqs. (1) and (2) plus the Coulomb interaction. As in the compositional superlattice, the effective energy gaps of heavy and light holes in n-i-p-i superlattices decrease as L increases. However, the effective energy gaps for two types of superlattices have different kinds of dependencies on L. For compositional superlattices, the energy difference between the edges of quantum wells of electrons and holes is fixed, which is the energy gap of GaAs material for GaAs-$Ga_{1-x}Al_xAs$ superlattices, and so the variation with L in effective energy gap is only due to the shift in energy levels of electrons and holes (relative to the bottom of quantum wells). For n-i-p-i doping superlattices, however, the variation in effective energy gap with L is caused by two factors. One is the amplitude of the space-charge potential increasing as L gets large, which causes the energy difference between the minima of potential wells of electrons and holes to decrease, and thus decreases the effective energy gaps. Another factor is that the ground-state energy levels of electrons and holes (relative to the bottom of the potential well) increase as L increases, which is also the consequence of increasing the space-charge potential amplitudes (the effect of energy levels decreasing due to quantum well width increasing is small). The latter affects the heavy and light holes differently since the effective energy gap of the heavy holes decreases more quickly as shown in Fig. 4. The effective energy gap obtained here is smaller than that obtained from the harmonic-oscillator-type potential approximation,[4] since the energy levels of electrons and holes relative to the bottom of potential wells under that approximation are independent with L. As seen from Fig. 4, the splitting between heavy-hole and light-hole effective energy gaps is small (in the order of a few meV). However, this splitting increases with L, in contrast to the results obtained for the GaAs-$Ga_{1-x}Al_xAs$ compositional superlattice ($x=0.3$ and well width a is equal to barrier width b), in which the splitting was in the order of a few tens of meV and decreases as L increases.[23] We attribute this to the fact that for compositional superlattices ($a=b=L/2$), the relative confinements of electrons and holes decrease as L increases and thus the energy levels of holes move closer to the bottom of the quantum wells. Since this effect on the light hole is more pronounced, as a result, the splitting between effective energy gaps decreases as L increases. For doping superlattices, however, the potential height increases as L increases, and therefore, the energy levels of holes move away from the bottom of the potential wells. Since this effect on the light hole is larger, as a result, the splitting between effective energy gaps of heavy and light holes increases with increasing L.

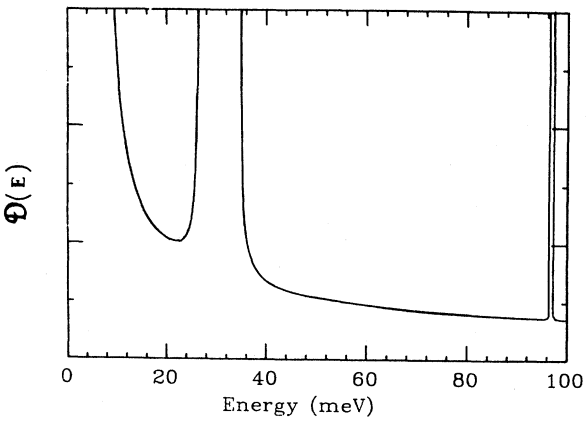

FIG. 5. Density of states of n-i-p-i doping superlattice with $n_D=n_A=10^{18}$ cm^{-3}, $d_i=d_n=d_p=L/4$, and $L=160$ Å.

We have also calculated the density of states $D(E)$, the number of states in the energy interval $E\rightarrow E+dE$, from the dispersion relation of Eq. (10). For one-dimensional systems, we have

$$D(E)=\frac{L}{\pi}\frac{dk}{dE}=\frac{(L/\pi)}{\left[\frac{dE}{dk}\right]} . \tag{11}$$

Figure 5 is a plot of the density of states $D(E)$ (arbitrary units) of the n-i-p-i doping superlattice at $n_D=n_A=10^{18}$ cm^{-3}, $d_i=d_n=d_p=L/4$, and $L=160$ Å. As for compositional superlattices, there are singularities in $D(E)$ near the center of the band and the edge of the band, where the dispersion in $E(k)$ is nearly horizontal. The minima

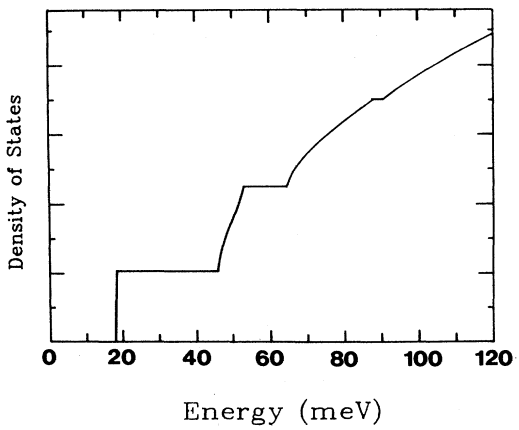

FIG. 6. Integrated density of states of n-i-p-i doping superlattice with $n_D=n_A=10^{18}$ cm^{-3}, $d_i=d_n=d_p=L/4$, and $L=300$ Å.

of $D(E)$ occur in places near the middle of minibands ($qL=0.5\pi$ etc.). Figure 5 also reflects new features in miniband structures. We can see that $D(E)$ for different energy levels are separated by minigaps. Figure 5 is very useful for interpreting experimental results in optical absorption and recombination processes. For absorption, the process takes place predominantly near the center of band and the edge of band, where more states are available. However, the center of the band is much more important for absorption compared with the edge of the band. This is because $D(E)$ near the center of the band region is less steep than at the edge of the band region. This effect is especially pronounced for the first conduction band.

Figure 6 is a plot of the integrated density of states, $N(E)=\int_0^E D(E')dE'$, of the n-i-p-i doping superlattice at $n_d=n_A=10^{18}$ cm^{-3}, and $d_i=d_n=d_p=L/4$ and $L=300$ Å. Many essential differences between the short- and long-period doping superlattices can be deduced from the results shown in Fig. 6. First, for long-period doping superlattices, $N(E)$ increases stepwise,[3] while for short-period doping superlattices, the increase in $N(E)$ differs from stepwise because of the dispersion in energy. This becomes more clear for higher conduction minibands. Second, the number of the density of states $N(E)$ for each band is different, and increases with increasing n, the band index. For large-period doping superlattices, however, dispersion in each energy band vanishes, and the number of the density of states, $N(E)$, is the same for each level, which is $m_e^*/\pi\hbar^2$, where m_e^* denotes the effective mass of the electron.[3] From Fig. 6, the relative values of the density of states for the first three conduction bands are $N_1(E):N_2(E):N_3(E)=1:1.17:1.24$. Figure 6 also shows the miniband widths and band gaps as already discussed from the dispersion relations.

IV. CONCLUSION

By using the multistep-potential approach and the matrix-transfer method, we have calculated the dispersion and miniband structure of n-i-p-i compensated doping superlattices of small periods. Dependence on both period length and doping concentration has been discussed. The effective energy gaps of heavy and light holes were also investigated. The densities of states of conduction subbands were obtained from the dispersion relation. The novel properties of small period n-i-p-i doping superlattices have been explored, and compared with properties of compositional superlattices as well as n-i-p-i superlattices of long periods. With some modifications, this multistep-approach method may also be used to calculated the band structure of uncompensated n-i-p-i doping superlattices. The results obtained here are useful both in basic research and device applications, especially for investigations of processes such as optical absorption, energy transformation, and recombinations in n-i-p-i doping superlattices.

*To whom all correspondence should be addressed.

[1]L. Esaki, J. Phys. (Paris) Colloq. **48**, C5-1 (1987).
[2]L. Esaki, IEEE, J. Quantum Electron **QE-22**, 1611 (1986).
[3]P. Ruden and G. H. Döhler, Phys. Rev. B **27**, 3538 (1983).
[4]K. Ploog and G. H. Dohler, Adv. Phys. **32**, 285 (1983).
[5]G. H. Döhler, Phys. Scr. **24**, 430 (1981).
[6]M. Gal, J. M. Viner, P. C. Taylor, J. S. Yaun, and G. B. Stringfellow, J. Vac. Technol. B **5**, 504 (1987).
[7]V. M. S. Gomes, A. S. Chaves, J. R. Leite, and J. M. Worlock, Phys. Rev. B **35**, 3984 (1987).
[8]E. F. Schubert, Y. Horikoshi, and K. Ploog, Phys. Rev. B **32**, 1085 (1985).
[9]E. F. Schubert, J. E. Cunningham and W. T. Tsang, Phys. Rev. B **36**, 1348 (1987).
[10]H. Yan and H. X. Jiang, Phys. Rev. B **37**, 6425 (1988).
[11]A. Harwit, J. S. Harris, Jr., and A. Kapitulnik, J. Appl. Phys. **60**, 3211 (1986).
[12]W. W. Lui and M. Fukuma, J. Appl. Phys. **60**, 1555 (1986).
[13]Y. Ando and T. Itoh, J. Appl. Phys. **61**, 1497 (1987).
[14]E. Merzbacher, *Quantum Mechanics*, 2nd ed. (Wiley, New York, 1970), pp. 73–105.
[15]R. L. Greene and K. K. Bajaj, Phys. Rev. B **31**, 913 (1984).
[16]*Numerical Data and Functional Relationship in Science and Technology*, Vol. 17 of *Landolt-Börnstein, New Series*, edited by O. Madelung (Springer, Berlin, 1982).
[17]W. T. Masselink, Y. C. Chang, and H. Morkoç, Phys. Rev. B **28**, 7373 (1983).
[18]H. J. Lee, L. Y. Juravel, J. C. Wooley, and A. J. SpringThorpe, Phys. Rev. B **21**, 659 (1980).
[19]R. C. Miller, A. C. Gossard, D. A. Kleinman, and O. Munteanu, Phys. Rev. B **29**, 3740 (1984).
[20]R. C. Miller, D. A. Kleinman, and A. C. Gosard, Phys. Rev. **29**, 7085 (1984).
[21]Y. Masumoto, S. Tarucha, and H. J. Okamoto, Phys. Soc. Jpn. **55**, 57 (1986).
[22]H. Weinert, F. Henneberg, V. Woggen, I. N. Uraltsev, and H. G. Bruhl, Phys. Scr. **35**, 76 (1987).
[23]H. X. Jaing and J. Y. Lin, Superlatt. Microstruct. **3**, 689 (1987).